Paper Review Topic: Magneto-Electric coupling in $BiFeO_3$

With Prof. Beatriz Noheda.
Student number: S2691140.

Abstract

Among the different types of multiferroic compounds, bismuth ferrite ($BiFeO_3$; BFO) stands out because it is perhaps the only one being simultaneously magnetic and strongly ferroelectric at room temperature. Therefore, in the past decade or more, extensive research has been devoted to BFO-based materials in a variety of different forms, including ceramic bulks, thin films and nanostructures. Ceramic bulk BFO doped with other metal elements at Bi or Fe site show excellent ferroelectric and piezoelectric properties and are thus promising candidates for lead-free ferroelectric and piezoelectric devices. BFO thin films, on the other hand, exhibit versatile structures and many intriguing properties, the inherent magnetoelectric coupling. BFO-based nanostructures are of great interest owing to their size effect-induced structural modification and enhancement in various functional behaviors, such as magnetic properties. Here, we provide an updated comprehensive review and our results on the BFO-based materials in the different forms of ceramic bulks, thin films and nanostructures, focusing on the pathways to modify different structures and to achieve enhanced magneto-electric properties.

Table of contents

1.Introduction

In recent years materials that exhibit both magnetic and electrical properties have become a hot topic of research. Novel devices can be created if there is the link between magnetic and electric properties and if magnetic and electric order can be controlled together. As we know magnetic and electric interactions couple to each other by the Maxwell equations that relate electric and magnetic fields, charge density and current density. The formal equivalence of the equations of electrostatics and magnetostatics explains numerous similarities in the theory of ferroelectrics and ferromagnets, for instance their behavior in external fields (Fig. 1) and domain structures (Fig. 2).

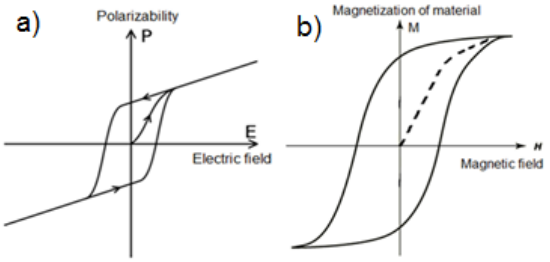

Figure 1. Typical (a) ferroelectric hysteresis loop. (b) ferromagnetic hysteresis loop.[1]

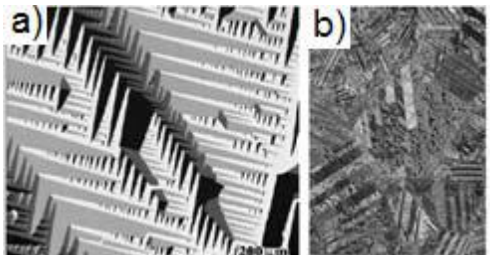

Figure 2. (a) Magnetic domains of Fe (100) [1]. (b) Ferroelectric domains in NaKNbO3 [2].

Magnetism appears in materials which have incomplete ionic d shells whereas ferroelectricity originates from atomic shifts that break inversion symmetry in a crystal.
Multiferroic materials possess two or more primary ferroic properties in the same phase. However, today the definition of multiferroics has been expanded to include other long-range orders, for instance antiferromagnetism (Fig. 3). Thus, any material that combines more than one of these properties is described as multiferroic. Nowadays, multiferroism often refers to a combination of ferroelectricity and magnetism (ferromagnetism, antiferromagnetism) in one particular material. Magnetoelectric switching can only be done if the magnetization and polarization are strongly coupled, which is a very unusual phenomenon. In 1959 Landau and Lifshitz pointed out the theoretical possibility of coupling magnetic and electric degrees freedom in one material [3]. Such materials have magnetization that is proportional to an applied electric field and polarization proportional to magnetic field. Later, Dzyaloshinskii predicted [4] and Astrov observed [5] this type of coupling, which is now known as the linear magnetoelectric effect. The next step was an attempt to create a novel material possessing at least two types of ordering – ferromagnetism and ferroelectricity. This was achieved by Soviet scientists [6]. However, the study of multiferroic meterial was virtually stopped soon afterwards. It should be noted that only very few multiferroics are linear magnetoelectrics (there are strict crystal symmetry requirements), and higher-order coupling terms usually dominate.

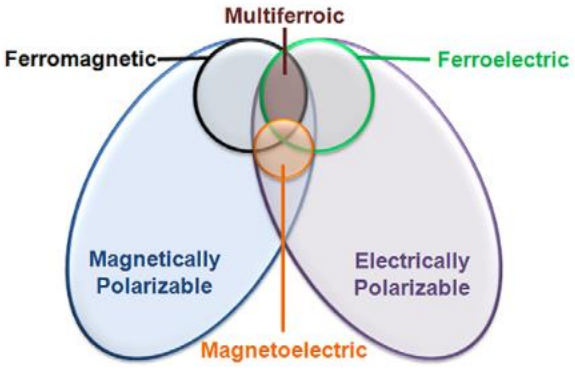

Figure 3. Multiferroics combine the properties of ferroelectrics and magnets [7].

Materials with pronounced magnetic and electronic properties permeate everywhere in modern technology and life. The current trend towards device miniaturization has led to interest in combining electronic and magnetic properties into multifunctional, multiferroic materials. The magnetoelectric effect would form the basis of a new type of devices for electric field-controlled magnetic memory data storage. Multiferroics are attractive not only because they have the properties of both magnetic and ferroelectric compounds, but also because the magnetoelectric coupling leads to additional functionality. However, the application of these materials is still a big question because the magnetoelectric coupling is too weak, making it very difficult to perform switching; furthermore, the polarization or magnetization are often too small and the temperatures at which these types of ordering occur are too low. Therefore, the development of new materials is very necessary.
One of the most studied and promising multiferroic materials to date is bismuth ferrite ($BiFeO_3$), which has a relatively simple structure and at the same time uncommon properties bismuth ferrite possesses two coupled order parameters ferroelectricity and antiferromagnetism at room temperature [8, 9]. Moreover, bismuth ferrite sets a standard in the global search for new multiferroic materials. Nevertheless, even in bismuth ferrite the magnetoelectric coupling is weak. However, in 2003, firstly Ramesh's group successfully created epitaxial $BiFeO_3$ multiferroic thin film heterostructures [10] that possess greatly enhanced multiferroic properties. These films display a room temperature spontaneous polarization that is almost an order of magnitude higher than that of the bulk. Therefore, the creation and development of artificial nanoscale structures is very promising. Thus, multiferroic materials hold the future for ultimate nano devices and are hence very interesting for theoretical and practical research, especially in nanoscience.

2. Brief theory

The first section of the current chapter present briefly the structure of BFO and then theories of ferroelectricity as well as ferromagnetism, magneto electric coupling. The last part is focused on the magneto-electric coupling in bulk, nano and thin films.

2.1. Structure and properties of $BiFeO_3$

$BiFeO_3$ is rhombohedrally distorted perovskite structure (Fig. 4) with R3c space group at room temperature. In the lattice Bi^{3+} ion occupy the corner position, Fe^{3+} in the body centered position, and O^{2-} in all face centered position.

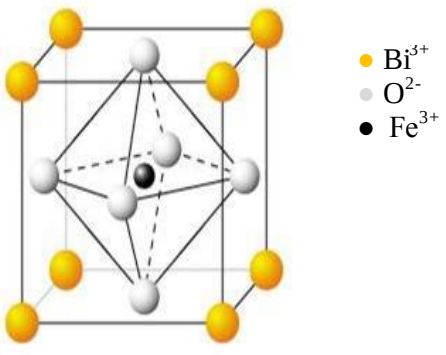

Figure 4. BiFeO3 having Perovskite structure [2].

The perovskite $BiFeO_3$ (BFO) was first produced in the late 1950s. The extended structure in crystal is represented in (Fig. 5).

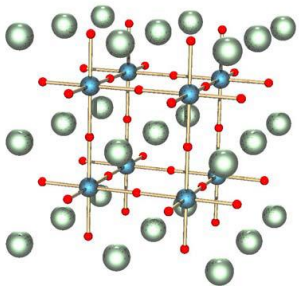

Figure 5. Extended view of ABX3 [2].

Structure of a perovskite with chemical formula ABX3 is shown in (Fig. 5). The red spheres are X atoms (usually oxygen), the blue spheres are B-atoms and the green spheres are A atoms. BFO unit cell can be described by pseudo-cubic, rhombohedral or hexagonal settings, where [111]pc ‖ [111]rh ‖ [001]hx with lattice parameters a_{pc} = 3.965 Å, α_{pc} = 89.35° for the pseudo-cubic unit cell (containing one formula unit) [11, 12], a_{rh} = 5.6343 Å and α_{rh} = 59.348 Å in the rhombohedral unit cell (containing two formula units), or a_{hex} = 5.578 Å and c_{hex} = 13.868 Å (containing six formula units) [11]

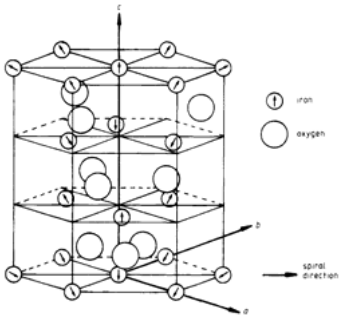

Figure 7. The part of the BiFeO3 lattice with only iron and oxygen ions shown. The arrows indicate the Fe3+ moment direction [13].

Sosnowska [13] studied the BFO magnetic structure and showed that each Fe3+ spin is surrounded by six anti parallel spins on the nearest Fe neighbors (Fig. 7) a G-type antiferromagnet. This means that the Fe magnetic moments are coupled ferromagnetically within the pseudocubic (111) planes and antiferromagnetically between adjacent planes.

However, it was also found that the BFO antiferromagnetic spin structure is modified by a long-range (620 ± 20 Å periodicity) modulation leading to a spiral modulated spin structure (SMSS) (Fig. 8) with a spiral direction of –[110] and a spin rotation plane of (110) [13-15].

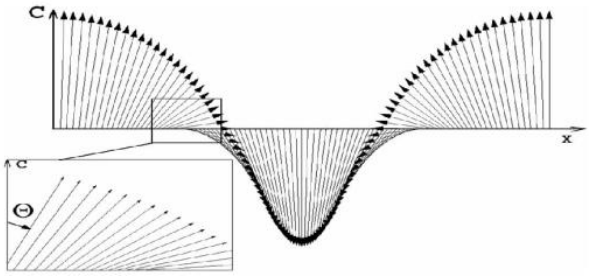

Figure 8. Schematic antiferromagnetic structure of BiFeO3 [14].

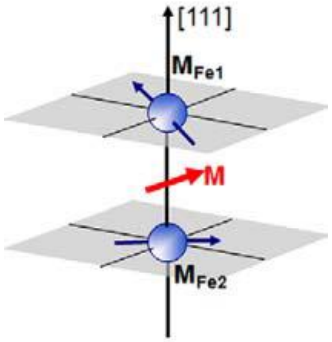

Figure 9. BFO might possess a weak ferromagnetic moment [16]

The SMSS leads to cancellation of any macroscopic magnetization. The linear magneto-electric effect is allowed by the average R3c point group but at the same time it is excluded by the SMSS. Instead, the SMSS allows the quadratic (second-order) magnetoelectric effect. The domain walls of BFO might show a weak ferromagnetic moment (according to Dzyaloshinski-Moriya theory) if the moments are oriented in a direction perpendicular to [111] (Fig. 9) [16]. However This theory [17, 18] has not been proved yet.

2.2. Ferroelectric Properties in $BiFeO_3$

The ferroelectric properties of BFO originate from A-site ions (Bi^{3+}). Bi^{3+} ions have an active lone pair (two valance electrons) capable of participating in chemical bonds using sp2 hybridized states but they do not participate in such bonding. The stereochemically active *6s2* lone pair causes the Bi 6p (empty) orbital to come closer in energy to the O 2p orbitals. This leads to hybridization between the Bi 6p and O 2p orbitals and drives the off-centering of the cation towards the neighboring anion resulting in ferroelectricity. So the B-site cation (Fe3+) lowers its energy by shifting along one of the [111] directions. Hence the direction of ferroelectric polarization in bulk BFO is along [001]*hexagonal*/[111]*pseudocubic* of the perovskite structure.

Early measurements of bulk ferroelectricity in the 1960s and 1970s yielded only small values of the polarization. Teague et al. [19] claimed that this small value of *P* was due to the leakage current in BFO and the actual polarization value of BFO should be an order of magnitude higher. This explanation was later verified [20]. The large polarization of the BFO thin films was initially thought to be due to strain enhancement [21], but later results showed that good single crystals also showed large remanent polarization values of 60 μC/cm2 along

the direction normal to (001) and, therefore, approximately 100 μC/cm2 along [111] pseudocubic [22]. Ab initio calculations also agreed with the obtained results [23]. These studies revealed that the major problem in the BFO films is their low resistivity and high leakage, caused by defects and nonstoichiometric compositions in the BFO materials. Considerable attempts also have been made to enhance the ferroelectric properties of BFO via ion substitution/co-doping A/B-sites [24].

2.3. Dzyaloshinskii-Moriya (DM) Interaction

The DM interaction is a process similar to superexchange, where the intermediate process is via spin-orbit interaction rather than an oxygen ion. Here the excited state is not connected with oxygen but is produced by spin-orbit interaction in one of the magnetic ions. It is an antisymmetric exchange interaction and is a contribution to the total magnetic exchange interaction between two neighboring magnetic spins S_i and S_j. The effect of DM in magnetically ordered systems is to provide spin canting of otherwise (anti) parallel aligned magnetic moment and thus, e.g. is a source of weak ferromagnetic behavior in an antiferromagnet. The DM exchange interaction occurs between the excited state of a magnetic ion and the ground state of the neighboring ion. For spin S_i and S_j. Mathematically it is written as

$$H_{DM}=D_{ij}.(S_i x S_j)$$

and is known as Dzyaloshinskii-Moriya interaction. In this equation H_{DM} is the Hamiltonian and D_{ij} is the DM vector and its orientation is constrained by symmetry. The D_{ij} vector is finite when the crystal field does not have inversion symmetry with respect to the center between *Si* and *Sj*. The form of the interaction is such that it tries to force S_i and S_j to be at right angles in a plane perpendicular to the vector D_{ij} in such an orientation as to ensure that the energy is negative. Its effect is therefore very often to cant (i.e. slightly rotate) the spins by small angles. It is found in, for example, α-$Fe2O_3$, $MnCO_3$, $CoCO_3$, and $BiFeO_3$ etc.

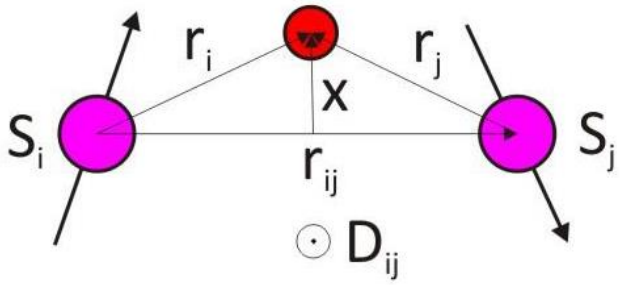

Figure 12: Determination of the orientation of the Dzyaloshinskii-Moriya (DM) vector from the local geometry [17].

The antisymmetric exchange is of importance for the understanding of magnetism induced electric polarization in a recently discovered class of multiferroics. Here, small shifts of the ligand ions can be induced by magnetic ordering, because the system tends to enhance the magnetic interaction energy on the cost of lattice energy. This mechanism is called "inverse Dzyaloshinskii-Moriya effect". In certain magnetic structures, all ligand ions are shifted into the same direction, leading to a net electric polarization.

2.4. Magnetic Properties of $BiFeO_3$

Magnetic properties of bulk BFO have been studied for many years. Sosnowska et al. [25] studied the BFO magnetic structure and showed that below its Néel temperature ($TN \sim 643K$), BFO has a G-type antiferromagnetic configuration. In G-type structure each Fe^{3+} with spin-up is surrounded by six of the nearest Fe neighbors with spin down. In Fe^{3+} there are five spins which are aligned in a half filled 3d shell. The Fe^{3+} magnetic moments are coupled ferromagnetically within the pseudocubic (111) planes and antiferromagnetically between adjacent planes. The antiferromagnetic order of BFO is oriented in the [001]h/[111]c direction and the spin rotation plane is parallel to the [110]h. A schematic diagram of the spin rotation and the spiral direction is shown in (Fig. 10).

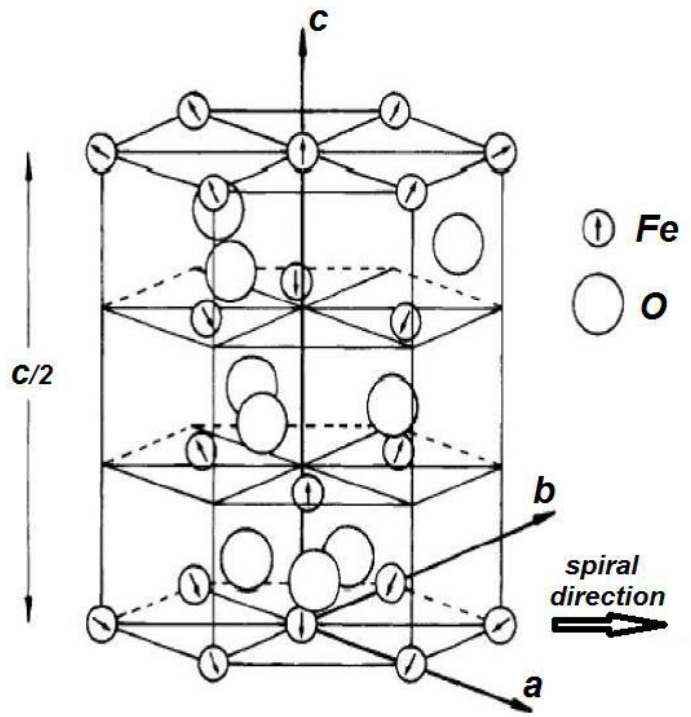

Figure 10: The part of the BiFeO3 lattice in hexagonal frame of reference with only iron and oxygen ions shown. The arrows indicate the Fe3+ moment direction. Figure from Sosnowska et al [25].

Tilting of the FeO_6 octahedra reduces the Fe−O−Fe angle from 180°, reducing the overlap of Fe d and O 2p orbitals. At ambient temperature and pressure the Fe−O−Fe angle is 154−156°. If the Fe−O−Fe angle was 180° one would expect collinear antiferromagnetism. It was also noted that if the moments were oriented perpendicular to the <111> polarization direction, the symmetry also permits a small canting of the moments resulting in a weak ferromagnetic moment due to the Dzyaloshinskii-Moriya (DM) effect (Fig. 11 (a)) [26-28]. On a local scale, BFO thus possesses both ferroelectric polarization and a weak ferromagnetic moment [29, 30]. However, the G-type antiferromagnetic structure of BFO is not homogeneous and is modulated to a spiral spin structure with a spiral direction of [110] and a spin rotation plane of (110). The modulation vector has a long period of $\lambda = 620-640$ Å [25]. The spiral modulated spin structure leads to the cancellation of any macroscopic magnetization as shown in Fig. 11(b) [25].

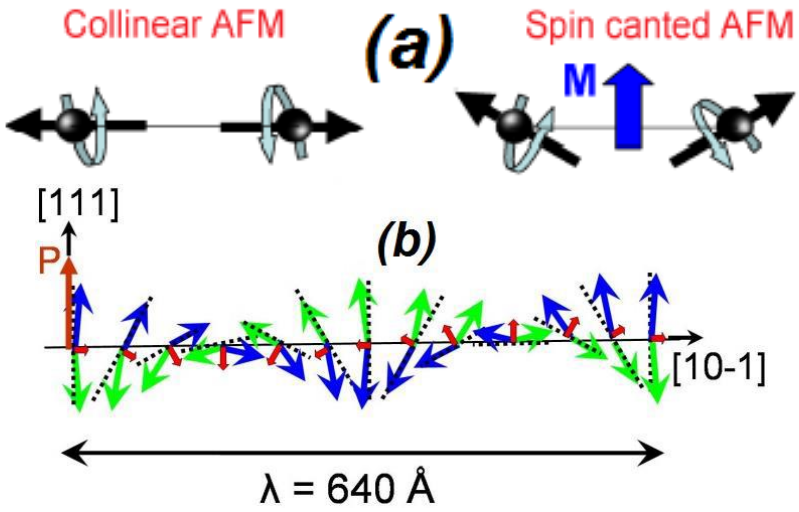

Figure 11: (a) Weak ferromagnetic moment induced by canted spin sublattices caused by the Dzyaloshinskii-Moriya (DM) interaction, (b) Schematic representation of the spin cycloid. The canted antiferromagnetic spins (blow and green arrows) give rise to a net magnetic moment (purple arrows) that is specially averaged out to zero due to the cycloid rotation [25].

The spiral spin structure is known to be suppressed by the factors such as (a) the application of high magnetic field (> 18 T) [31] (b) the application of external stress or due to epitaxial constraints in thin films [32] (c) finite size effects in nanosized BFO [33] and (d) the imposition of structural modifications introduced by appropriate cationic substitution [34, 35]. Several attempts have been made to create net magnetization in BFO, with some efforts focusing on the possibility of using chemical substitution to "unwind" the spiral spin structure and extract the canted magnetic moment.

2.5. Theoretical Study of Magnetoelectric (ME) Effect

As already discussed that from an application standpoint, the real interest in multiferroic materials lies in the possibility of strong ME coupling. ME effects include both linear and non-linear responses to an external electric or magnetic field which can be mathematically expressed by an expansion of free energy of a material,

$$F(E,H) = F_0 - P^s_i E_i^s - M^S_i H_i^s - 1/2\,\varepsilon_0\varepsilon_{ij} E_i E_j - 1/2\mu_0\mu_{ij} H_i H_j - 1/2\beta_{ijk} E_i H_j H_k - 1/2\gamma_{ijk} H_i E_j E_k - \cdots \quad (1)$$

with E and H as the electric field and magnetic field respectively. Differentiation leads to both polarization and magnetization.

$$P_i(E,H) = -(\partial F/\partial E_i) = P^S_i + \varepsilon_0\varepsilon_{ij} E_j + \alpha_{ij} H_j + 1/2\beta_{ijk} H_j H_k + \gamma_{ijk} H_i E_j + \cdots \quad (2)$$

$$M_i(E,H) = -(\partial F/\partial H_i) = M^S_i + \mu_0\mu_{ij} H_j + \alpha_{ij} E_i + \beta_{ijk} E_i H_j + 1/2\gamma_{ijk} E_j E_k + \cdots \quad (3)$$

where F is the free energy of the material, P is the electric polarization, M is the magnetization, E and H are the electric and magnetic fields, respectively. P^S and M^S are spontaneous polarization and magnetization, respectively. ε and μ are the electric and magnetic susceptibilities, respectively. α is the induction of polarization by a magnetic field (or induction of magnetization by electric field) and is known as linear magnetoelectric effect.

Higher order magnetoelectric effects such as β and γ also exist but much smaller in magnitudes [36].

3.Fabrication and properties of $BiFeO_3$

3.1. Ceramic, Thin films and Nanoparticles, nanopowders

Several techniques have been developed to fabricate BFO ceramic bulks to overcome the issues such as the formation of secondary phases as well as the occurrence of high leakage current. When BFO bulks are prepared by the conventional solid-state reaction method using oxides as the starting materials, a large number of extra unexpected phases ($Bi_2Fe_4O_9$, $Bi_{25}FeO_4$, Bi_2O_3) can be easily formed. Wet chemical methods and the use of proper oxide precursors could effectively suppress the formation of secondary phases and we can improve the quality of overall microstructures. In addition to the conventional sintering, liquid phase sintering and spark-plasma sintering have also been explored. Techniques of preparing single crystals have been investigated.

As it is well known that certain secondary phases (e.g., $Bi_{25}FeO_{40}$ and $Bi_2Fe_4O_9$) are easy to form in both undoped and doped-BFO ceramics prepared by the conventional solid-state reaction method [37,38]. Due to the high conductivity of these extra secondary phases, a properly saturated *P-E* loop cannot be attained and the ceramics cannot be fully poled. It is necessary to fabricate a high-resistivity BFO ceramic in order to further investigate the electrical properties. One attempt was to leach the impurity phases with dilute nitric acid [39]. Unfortunately, the as-prepared samples thus prepared showed poor ferroelectric loops due to the low density. It was reported that the liquid phase technique could be used to sinter the dense BFO ceramics [40-45]. As a result, the chemical modifications and preparation methods for BFO ceramic bulks are made so these can significantly affect the electrical and magnetic properties of BFO ceramic bulk. For improvement in electrical and magnetic properties, ion substitution is one of the most common approaches for BFO ceramic bulks, including substitutions at either Bi or Fe or both sites. the ion substitution for Bi site can also modify the ferroelectric, magnetic and piezoelectric properties and it also improves the leakage current [46-53].

As bulk $BiFeO_3$ is a room-temperature ferroelectric, it has a spontaneous electric polarization directed along one of the[111] directions of the perovskite structure. The spontaneous polarization is 3.5 μC/cm2 along the [100]direction and 6.1 μC/cm2 in the [111] direction at 77 K [54], which is smaller than expected for a material with such a high Curie temperature. Because the ferroelectric state is attributed to a large displacement of the Bi ions relative to the FeO_6 octahedra, this leads to the following important consequence. The ferroelectric polarization of BFO lies along the <111> direction, leading to the formation of eight possible polarization directions (positive and negative orientations long the four cube diagonals, $P_{i\pm}$ with i={1,4}) which correspond to four structural variants (Fig. 16)

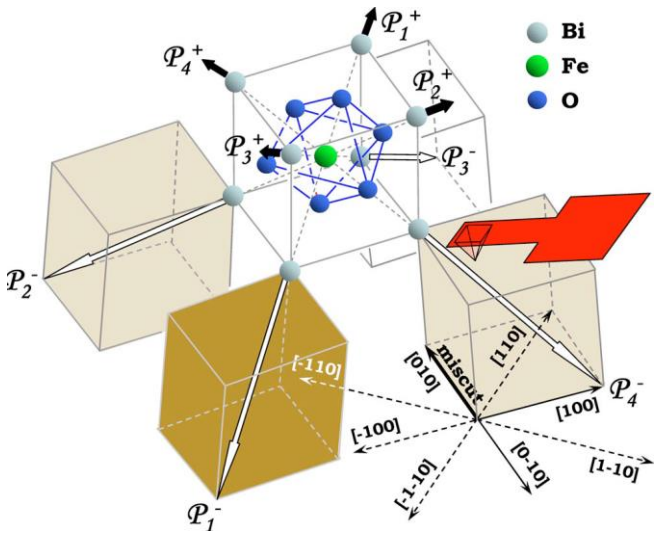

Figure 16. A schematic picture of the four different structural variants in (001) rhombohedral films. $P_{i\pm}$ {i=1,4} denote the polarization vectors. The central unit represents the perovskite building block of the rhombohedral structure [55].

It is evident from figure 16 that the direction of the polarization can be switched by 180°, 109°, and 71°, as shown in (Fig. 17) [55-57].

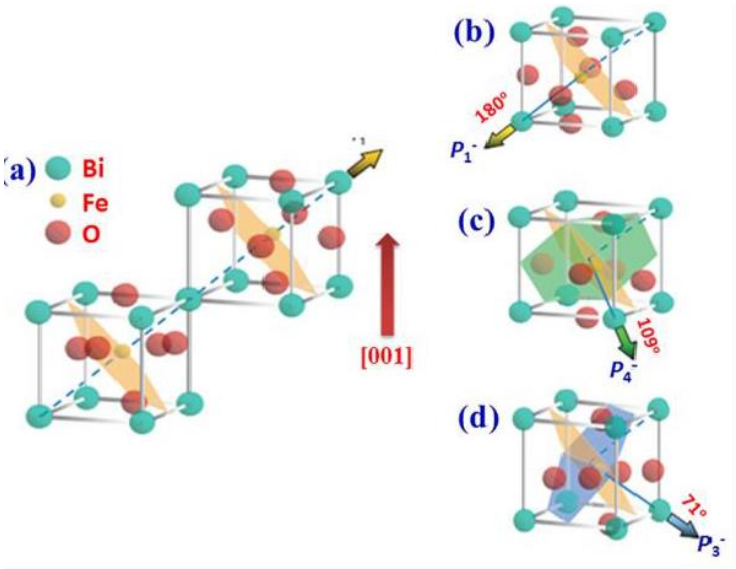

Figure 17. Schematic diagram of (001)-oriented BiFeO3 crystal structure and the ferroelectric polarization (bold arrows) and antiferromagnetic plane (shaded planes). (a) Polarization with an "up" out-of-plane component before electrical poling. (b) 180°, (c) 109°, and (d) 71° switching mechanisms [56].

Fig. 18, shows the resulting mosaic-like architecture with three types of domain walls for Ta/CoFe/BFO/STO structures with 71°,109° and 180° differences in their polarization directions.

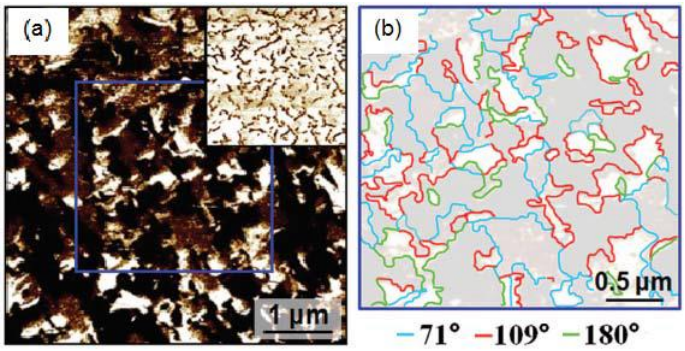

Figure 18. (a) In-plane and out-of-plane (inset) PFM contrast for typical BFO films that exhibit exchange bias. Detailed domain wall picure for (b) mosaic-like BFO films [58].

Here, Co0.9F0.1 (CoFe) was used to initiate exchange interactions between the ferromagnetic CoFe and the multiferroic, antiferromagnetic BFO. Six fold degeneracy forms in an effective easy magnetization plane oriented perpendicular to the [111] direction. This means that polarization switching by either 71° or 109° will lead to a change in orientation of the easy magnetization plane. Thus, ferroelectric switching leads to a reorientation of the antiferromagnetic order. Fig. 19 shows in-plane PFM images for a $BiFeO_3$ film deposited on conducting $SrTiO_3$ (100) substrates before and after electrical poling. Regions 1&2, 3, and 4 correspond to 109°, 71° and 180° switching respectively. According to figure 17, only 109° ferroelectric switching changes the in-plane projection of the ferroelectric and antiferromagnetic order parameters and therefore can be detected by PFM. That is why there is no change in contrast difference in regions 3 and 4 (Fig. 19). Thus, coupling between ferroelectricity and antiferromagnetism has been demonstrated in BFO thin films.

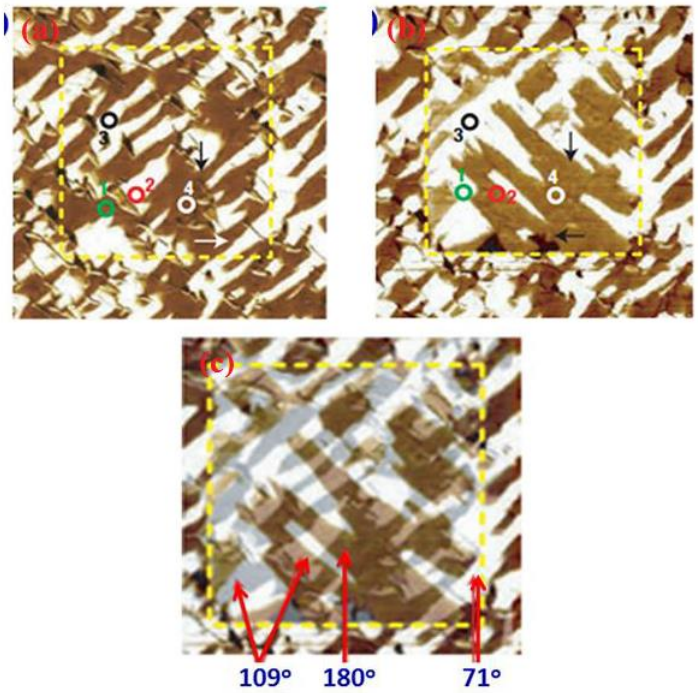

Figure 19. In-plane PFM images of 600-nm-thick BiFeO3 films before (a) and after (b) poling. The arrows show the direction of the in-plane component of ferroelectric polarization. Regions 1 and 2 (marked with green and red circles, respectively) correspond to 109° ferroelectric switching, whereas 3 (black and yellow circles) and 4

(white circles) correspond to 71° and 180° switching, respectively. In c used to identify the different switching mechanisms that appear with different colours and that are labeled in the figure [56].

In [59], the possibility of controlling the ferroelectric domain structure in bismuth ferrite films was demonstrated using vicinal $SrTiO_3$(STO) substrates. Single domain BFO films on such surfaces can be fabricated. Thus, the possibility of switching the magnetization plane opens a direct way to control the magnetic state using an electric field. Such a phenomenon has possible applications in magnetic memory devices.

As BFO-based materials have widely used in composites, bilayers, trilayers, and multilayered structures, consisting of both piezoelectric (ferroelectric) and magnetic phases, to achieve strong magneto-electric coupling at room temperature [60].

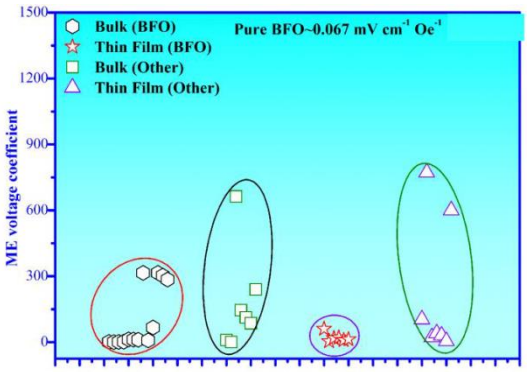

Figure. 20. Magnetoelectric properties of selected BFO materials (unit of ME coupling: mV cm-1 Oe-1) [60].

Fig. 20 shows the ME coefficients of BFO-based materials in comparison to other materials. The largest ME coupling of BFO-based materials was achieved in $0.3Co_{0.7}Zn_{0.3}Fe_2O_4$-$0.7Bi_{0.9}La_{0.1}FeO_3$ nanocomposites as reported by Yadav *et al* [61]. A maximum ME coefficient as high as 315 mV cm-1 Oe-1 at 50 kHz was obtained, due to the high piezomagnetic and piezoelectric coefficient induced by small grain sizes.

However, the ME coefficient of BFO-based materials is still inferior, compared with those of other materials [62,63].

For example, Nan *et al.*[62] prepared a Pt(30nm)/Pb($Zr_{0.52}Ti_{0.48}$)O_3(400nm)/Pt/Ni multiferroic film heterostructure, which showed a large αE31 of ~772 mVcm-1 Oe-1 at the low *dc* magnetic bias field of 86 Oe. Therefore, there is still a large scope to improve the ME coefficient of BFO-based materials. Perhaps forming nanocomposites consisting of a strong magnetic phase and BFO, in which the piezoelectric properties of BFO could be further enhanced, may lead to a high ME coefficient.

As reviewed above, the ferroelectric polarization and weak magnetization is coupled in single-phase BFO. This has also been confirmed by the first-principles density functional theory [64]. However, the magnetoelectric coupling coefficient of single-phase BFO is rather small, only ~0.067 mV cm-1 Oe-1 at ~9.5 kOe [65]. Kimura *et al.* recently [66] showed that the ME coupling of BFO at RT could be enhanced by the strategies such as:

(a) destroying the long range spin cycloid, and/or (b) shifting the transition temperature *T*C or *T*N toward room temperature. Other attempts were made to enhance the ME coupling in BFO by: (i) construction of layered or nanosized bulk composites or multiferroic film heterostructures;[67-76] (ii) chemical substitution with diamagnetic (Ca2+, Sr2+, Ba2+), rare earth (La3+, Gd3+, Nd3+, Dy3+, Sm3+) elements at the A-site, and magnetic (Mn3+, Cr3+), non-magnetic dopant (Zr4+, Ti4 elements at B-site;[77-81] (iii) formation of BFO solid solutions with other compounds;[82-85] and (iv) development of BFO nanoparticles with crystallite size less than the periodicity of helical order via various chemical routes [86,87]. Here we would discuss ME coupling in film heterostructures with application point of view.

In most of previous works, the electric field control of magnetism was realized in BFO/ferromagnet film heterostructures, where the ferromagnet materials were either oxides (e.g., $La_{0.7}Sr_{0.3}Mn_{0.95}$) or transitional metals (e.g., $Co_{0.9}Fe_{0.1}$. and Permalloy [88]. Advantage of the intrinsic ME coupling in BFO can be taken in these films heterostructures and the interface exchange coupling between BFO and the ferromagnetic layer. In BFO/LSMO films heterostructures, the exchange bias was reversibly switched between two stable states with opposite exchange bias polarities upon ferroelectric switching of BFO, as examined by magnetotransport measurements.[87] Unfortunately, this effect was only observed at <30 K. However, the electric field control of magnetization could be realized in BFO/$Co_{0.9}Fe_{0.1}$ film heterostructures at room temperature. The X-ray magnetic circular dichroism (XMCD)–photoemission electron microscopy (PEEM) revealed that the reversal of magnetization of $Co_{0.9}Fe_{0.1}$ was 90° [88] and which was later promoted to 180° [89]. But this is noticeable that applying the electric field with the in-plane electrode geometry, which may not be suitable for memory applications.

A very recent study successfully demonstrated that even by applying vertical electric fields, the 180° reversal of magnetization of $Co_{0.9}Fe_{0.1}$ could also be achieved.[98] By a combination of time-dependent, dual-frequency piezoresponse force microscopy (PFM) and first-principles calculations, authors in Ref. [90] demonstrated that the application of a vertical electric field induced two-step sequential rotation of polarization [Fig. 21(a)].

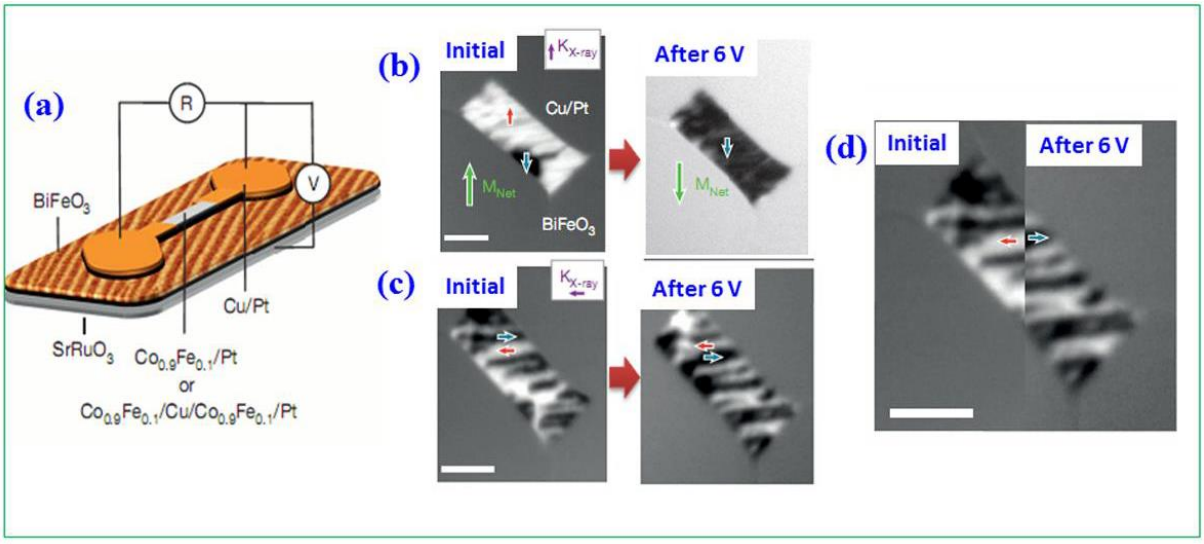

Figure. 21. (a) Magnetoelectric device consisting of Co0.9Fe0.1 or Co0.9Fe0.1/Cu/ Co0.9Fe0.1 spin value on BFO. Initial and final (after applying 6 V) directions of in-plane Co0.9Fe0.1 moments with components viewed (b) perpendicular and (c) parallele to the stripe domains. (d) Images of initial and final states merged near the centre of Co0.9Fe0.1, with the components viewed parallel to stripe domains [90].

Through the two-step switching and owing to the ME coupling, the Dzyaloshinskii–Moriya (DM) vector and weak ferromagnetism of BFO can be switched by 180°. As a result, the $Co_{0.9}Fe_{0.1}$ magnetization would in principle be reversed by 180° even by applying a vertical electric field. Then, the XMCD-PEEM technique was used to experimentally probe the magnetic moment change of $Co_{0.9}Fe_{0.1}$ induced by vertical electric field.As shown in Figs. 21(b) and (c), after the application of 6 V (10 ms) pulse, the net $Co_{0.9}Fe_{0.1}$ magnetization is switched by 180°. Moreover, the 180° electric-field induced reversal of $Co_{0.9}Fe_{0.1}$ moments within each domain can be clearly observed [Fig. 21(d)], confirming the coupling between the DM vector and ferroelectric polarization (which is theoretically pridicted). Although

substantial progress has been achieved in the electric field control of magnetism in BFO/ferromagnetic thin films and film hetrostructures, some important issues, e.g., switching reliability, still remain challenging.[91] Further studies are therefore of demand to validate the practical applications.

Due to the size effects on structure and functional properties, considerable efforts have been devoted to the controllable synthesis of low-dimensional BFO nanostructures with various morphologies. According to their dimensions, four types of BFO nanostructures can be defined: (i) zero dimension (nanoparticles or dots), (ii)one dimension (nanowires, nanorods, and nanotubes), (3) two dimension (thin films and nanoislands), (4) three dimension (nanocomposites consisting of nanowires, nanotubes arrays).Among those methods reported, two chemistry-based approaches (i.e., sol-gel and hydrothermal method) have been more commonly employed than others.[92-110] Indeed, a wide range of nano-morphologies have been developed by these techniques, including nanoparticles,[111,112-115, 93,116-120] nanocubes, nanotubes, nanowires, nanodots, nanosheet, nanoplate, and nanoislands.

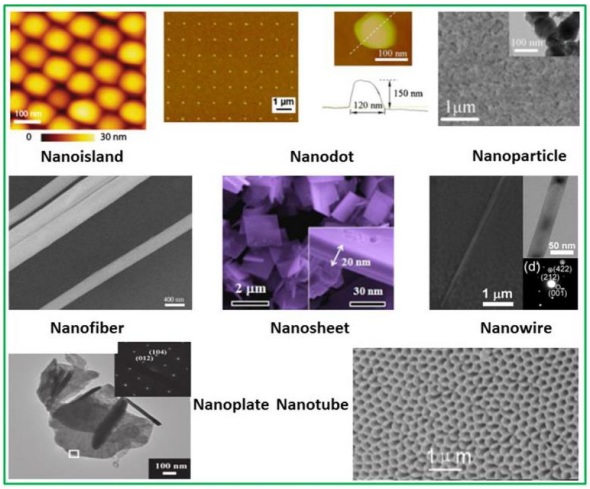

Figure.22. Selected examples of morphologies of BFO nanostructures [93, 94].

Fig. 22 shows selected examples of morphologies of BFO nanostructures prepared by different techniques [93,94]. These nanomorphologies can be well modulated by the processing technique and parameters chosen for fabrication.
Comparing to the forms of thin films or ceramic bulks, they possess stronger multiferroic behaviour,[121] depending on the corresponding morphological features.[122-126] Previous studies have also revealed the two major factors largely responsible for the enhanced magnetic properties in nano particles :[127]
(i) large degree of suppression of magnetic structure (period length of ~62 nm) with decrease in nanoparticle size, and (ii) uncompensated spins and strain anisotropies at surface.

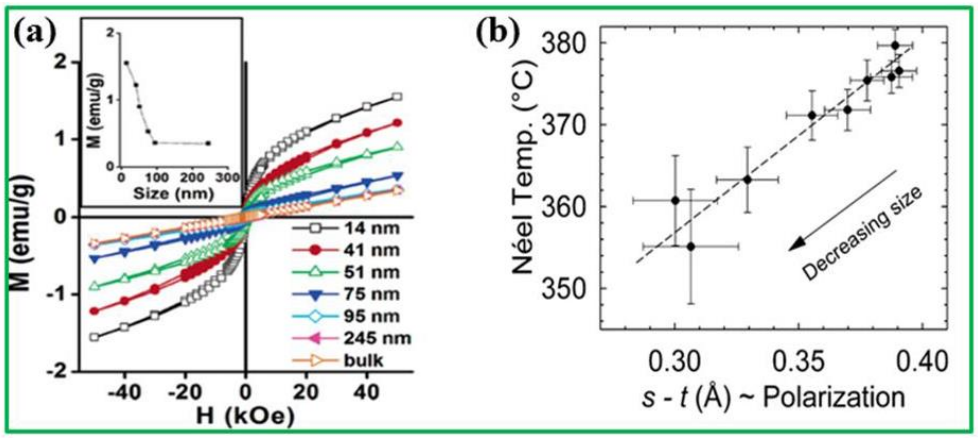

Figure. 23. (a) Size-dependent M-H loops at 300 K for BiFeO3 nanoparticles. (b) Strong size-dependent Néel temperature (*T*N) and polarization behavior of BiFeO3 nanoparticles [128].

Fig. 23(a) shows the size effect of *M-H* loops of BFO nanoparticles, measured at 300 K [128]. Compared with those of ceramic bulks, nanoparticles show better magnetic behavior. The magnetic response increases rapidly with the decrease in particle size.

In particular, there is a dramatic increase in *M*r for sizes below 62 nm (the period length of the spiralmodulated spin structure of BiFeO3) due to the modification in long range spiral-modulated spin structure [127]. It is seen from Fig. 23(b) that the decrease in size gives rise to a decrease of *T*N because of phenomenological scaling relations and possible correlations with decreasing polarization.[127]

Fig. 24 shows Electrical measurements carried out O (oxygen) annealed pelletized samples of nano sized BFO. dielectric measurements of BFO nanoparticles at high temperatures by using two probe setup are discussed by (Manzoor et al. 2012). Both the capacitance as well as dissipation factor (tangent loss) were recorded by using Wayne Kerr LCR meter bridge (WK4275).

Both the real part of the dielectric constant (ε) and the dissipation factor (tan d) are shown as functions of temperature for the different-sized particles. Figure 24a, b shows the temperature dependence of both dielectric constant and tangent loss samples. In addition to the usual decrease of the (ε) with decreasing temperature in the T\Tc region, anomalies observed in the dielectric data around T = 560 K for both (ε) and the tan d, respectively. This anomaly becomes more pronounced for the smaller-sized nanoparticles that have shown more magnetic. We note that the reported Neel temperature for bulk BFO is T_N = 643 K but lower values for the Neel temperature for nanoparticles are quite usual due to finite size effects. The dielectric anomaly around T_N = 560 K is therefore understood to be related to the development of the AFM (antiferromagnetic) to paramagnetic transition.

As at the same temperature the absence of complete compensation of the moment will lead to the weak ferromagnetism hence the anomaly in the (ε) is to be taken as a signature of the coupling between the electric polarization (P) and the magnetization (M), as expected in any multiferroic system. It is noticeable that the dielectric anomaly is largest for the smallest particles that also show the strongest ferromagnetic component, further supporting its origin as being due to the magneto-electric coupling [128].

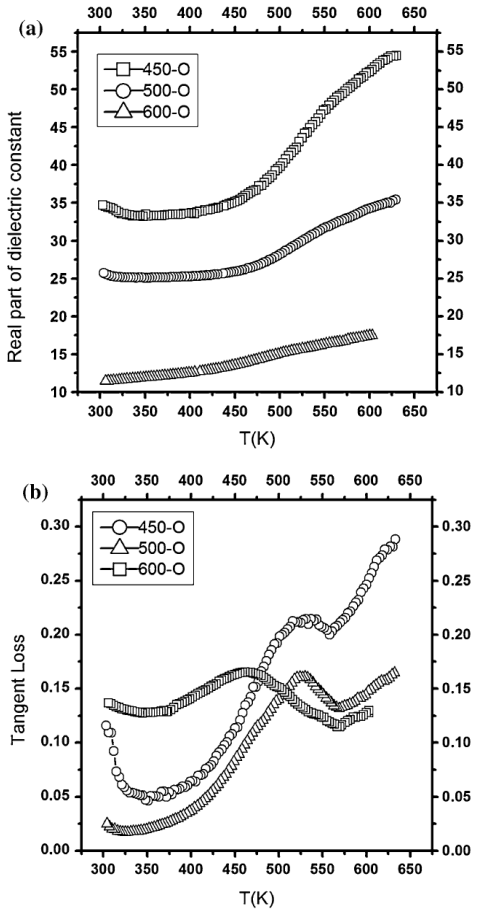

Figure. 24 (a)Temperature dependence of real part of dielectric constant at different temperatures. (b) Temperature dependence of tangent loss at various temperatures [129].

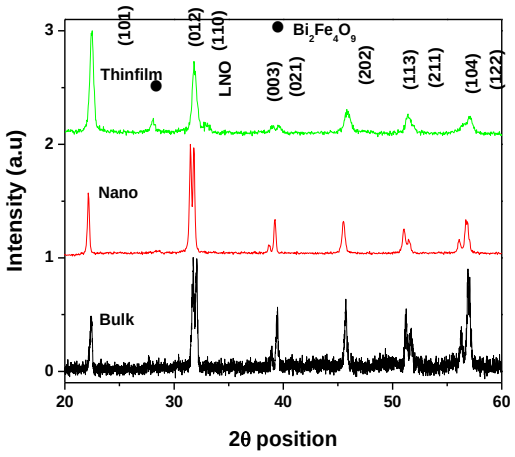

Figure. 25: XRD diffraction patterns of BFO for Bulk, Nanoparticles and Thin film, obtained at room temperature (not published yet).

Fig. 25 depicts the XRD patterns of Bulk, Nanoparticles and thin film of BFO at room temperature. No peak from residual secondary phases (Bi_2O_3, Fe_2O_3, $Bi_2Fe_4O_9$ and $Bi_{25}FeO_{39}$) was observed for bulk and nanoparticles but small amount of secondary phase ($Bi_2Fe_4O_9$) was observed in thin film at $2\theta \approx 28°$. In case of thin films a diffraction peak of LNO can also be

seen around 2θ = 32.78° which was used as buffer layer. The observed diffraction peaks correspond to rhombohedrally distorted perovskite structure (space group $R3c$).

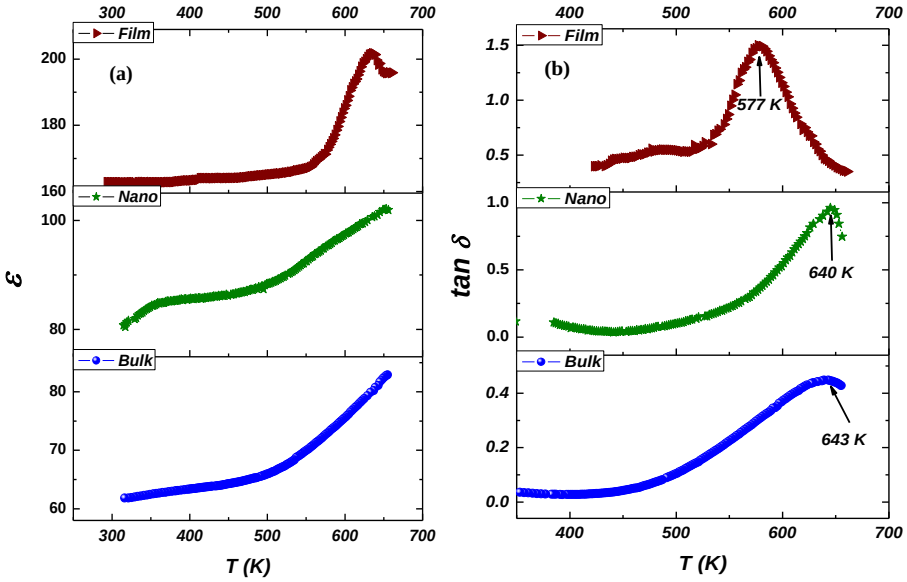

Figure. 26 (a) Plot of dielectric constant vs. temperature BFO for Bulk, Nanoparticles and Thin film, obtained at 100 kHz. (b) Plot of imaginary part of dielectric constant of BFO for Bulk, Nanoparticles and Thin film, obtained at 100 kHz. (not published yet).

The behavior of in phase part and out phase of dielectric constant with temperature for bulk, nanoparticles and thin films of BFO is shown in Fig. 26(a, b). It is observed that dielectric constant increases with increase in temperature in all these three systems. It has been reported that the Néel temperature (T_N) of BFO is 643 K (Hussain et al 2013). For the case of bulk and nano sized BFO, no anomaly in real part of dielectric constant is observed up to 650 K. However, for the case of thin film we can see the dielectric anomaly. This anomaly in the dielectric constant therefore signifies coupling between polarization (P) and magnetization (M), as expected in a multiferroic system (Ederer and Spaldin 2005). Fig. 26(b) shows the out of phase part (losses) of bulk, nanoparticles and thin films of BFO, respectively. A very pronounced dielectric anomaly can be noted in out of phase part, for the bulk, nanoparticles and thin film (Palker et al. 2002). These dielectric anomalies arise at 643 K, 640 K, and 577 K for Bulk, nanoparticles and thin films, respectively. A small decrease in Néel temperature (from 643 K for the case of bulk sample) for the case of nanoparticles is observed, but a larger decrease is found for thin films (Manzoor et al. 2012). For the case of nanoparticles and thin films, larger strains are expected that can affect the strength of the superexchange interaction and hence the Néel temperature. XRD results also supporting this argument. The comparison of the full width at half maximum (FWHM) of (101) peak near $2\theta \approx 22°$ shows that the peak is less broad in case bulk BFO. The FWHM of this peak increases in case of nanoparticles and it is largest in case thin film, implying the highest strain in thin film. The improvement of magnetic-electric properties in these systems is an encouraging sign for the development of practical application. these results indicate that thin films would be more suitable for multiferroic applications than bulk or nanoparticle based systems.

Conclusions

Development of multiferroic materials for different applications is one of the focus areas in functional materials research community. The investigations into multiferroic bismuth ferrite materials have seen great growth in the past fifteen years. In this review, we have visited the progress and magneto-electric coupling of the BFO-based materials in the different forms of ceramic bulks, thin films and nanostructures, where it is discussed that how we can enhance magneto-electric coupling and its application point of view. At the end of this review we presented our results on BFO in the form of bulk, nanoparticles and thin film which has been successfully synthesized and a comparison between the multiferroic properties has been made. XRD results suggest that bulk, nanoparticles and thin films crystallize in the rhombohedral structure. The Néel temperature is 643 K, 640 K and 577 K for bulk, nanoparticles and thin film, respectively, as evidenced by the presence of dielectric anomaly in the out of phase part of the dielectric constant. The improvement of magnetic-electric properties in these systems is an encouraging sign for the development of practical application. Our results indicate that thin films would be more suitable for multiferroic applications than bulk or nanoparticle based systems.

References

1. http://unit.aist.go.jp/ce-core/cerc/topicsE.html.
2. http://www.materials.manchester.ac.uk/.
3. L. D. Landau and E. M. Lifshitz, Electrodynamics of continuous media (Fizmatgiz, Moscow, (1959).
4. I. E. Dzyaloshinskii, Sov. Phys. JETP **10**, 628 (1959).
5. D. N. Astrov, Sov. Phys. JETP **11**, 708 (1609).
6. G. A. Smolenskii and I. E. Chupis, Sov. Phys. Usp. Vol. **25**, 475 (1982).
7. W. Eerenstein, N. D. Mathur & J. F. Scott, Nature Vol. **442**, 759-765 (2006).
8. J. R. Teague, R. Gerson and W.J. James, Sol. Stat. Commun. **8** 1073 (1970).
9. P. Fischer and M. Polomska, J. Phys. C: Sol. Stat. Vol.**13**, 1931 (1980).
10. J. Wang et al., Science **299**, 1719 (2003).
11. F. Kubel and H. Schmid, Acta Crystallographica Section B **46**, 698 (1990).
12. C. Michel, J.-M. Moreau, G. D. Achenbach, Robert Gerson and W. J. James, Solid State Communications **7**, 701 (1969).
13. I. Sosnowska et al., J. Phys. C. **15**, 4835 (1982).
14. A. M. Kadomtseva et al., Phase Transitions, Vol. **79**,1019-1042 (2006).
15. D. Lebeugle et al., Phys. Rev. B. **76**, 024116 (2007).
16. Moriya T., Phys. Rev. **120**, 91 (1960).
17. V. Raghavendra et al., Applied Physics Letters Vol. **94**, 082505 (2009).
18. T. Zhao et al., Nature Mater. Vol. **5**, 823 (2006).
19. J. R. Teague, R. Gerson and W. J. James, Solid State Communications **8**, 1073 (1970).
20. R. P. S. M. Lobo, R. L. Moreira, D. Lebeugle and D. Colson, Physical Review B **76**, 172105 (2007).
21. J. Wang, J. B. Neaton, H. Zheng, V. Nagarajan, S. B. Ogale, B. Liu, D. Viehland, V. Vaithyanathan, D. G. Schlom, U. V. Waghmare, N. A. Spaldin, K. M. Rabe, M. Wuttig and R. Ramesh, Science **299**, 1719 (2003).
22. D. Lebeugle, D. Colson, A. Forget and M. Viret, Applied Physics Letters **91**, 022907 (2007).
23. V. V. Lazenka, G. Zhang, J. Vanacken, I. I. Makoed, A. F. Ravinski and V. V. Moshchalkov, Journal of Physics D: Applied Physics **45**, 125002 (2012).
24. S. Y. Yang, J. Seidel, S. J. Byrnes, P. Shafer, C. H. Yang, M. D. Rossell, Y. Pu, Y. H.

Chu, J. F. Scott, J. W. Ager, L. W. Martin and R. Ramesh, Nature Nanotechnology **5**, 143 (2010).
25. I. Sosnowska, T. Peterlinneumaier and E. Steichele, Journal of Physics C-Solid State Physics **15**, 4835 (1982).
26. C. Ederer and C. J. Fennie, Journal of Physics: Condensed Matter **20**, 434219 (2008).
27. I. Dzyaloshinsky, Journal of Physics and Chemistry of Solids **4**, 241 (1958).
28. T. Moriya, Physical Review **120**, 91 (1960).
29. A. K. Z. Y. F. Popov, G. P. Vorobev, A. M. Kadomtseva, V. A. and Murashev and D. N. Rakov, JETP Lett **57**, (1993).
30. A. K. Z. A. M. Kadomtseva, Y. F. Popov, A. P. Pyatakov and G. P. Vorob'ev, G. P., JETP Lett **79**, (2004).
31. B. Ruette, S. Zvyagin, A. P. Pyatakov, A. Bush, J. F. Li, V. I. Belotelov, A. K. Zvezdin and D. Viehland, Physical Review B **69**, (2004).
32. J. Li, J. Wang, M. Wuttig, R. Ramesh, N. Wang, B. Ruette, A. P. Pyatakov, A. K. Zvezdin and D. Viehland, Applied Physics Letters **84**, 5261 (2004).
33. T.-J. Park, G. C. Papaefthymiou, A. J. Viescas, A. R. Moodenbaugh and S. S. Wong, Nano Letters **7**, 766 (2007).
34. V. R. Palkar, D. C. Kundaliya, S. K. Malik and S. Bhattacharya, Physical Review B **69**, (2004).
35. N. G. Wang, J. Cheng, A. Pyatakov, A. K. Zvezdin, J. F. Li, L. E. Cross and D. Viehland, Physical Review B **72**, (2005).
36. Y. P. Filippov, G. G. Ihas and V. V. Vainberg, Review of Scientific Instruments **80**, 094902 (2009).
37. Valant M, Axelsson AK, Alford N. Chem Mater;19:5431-6 (2007).
38. Morozov MI, Lomanova NA, Gusarov VV. Russ J Gen Chem;73:1676 (2003).
39. Kumar MM, Palkar VR, Srinivas K, Suryanarayana SV. Appl Phys Lett;76(19):2764-6 (2000).
40. Yu B, Li M, Liu J, Guo D, Pei L, Zhao X. J Phys D Appl Phys;41:065003 (2008).
41. Walker J, Budic B, Bryant P, Kurusingal V, Sorrell CC, Bencan A, Rojac T, Valanoor N. IEEE T Ultrason Ferr;62:83-7 (2015).
42. Wang YP, Zhou L, Zhang MF, Chen XY, Liu JM, Liu ZG. Appl Phys Lett;84:1731-3 (2004).
43. Yuan G L, Or SW. Appl Phys Lett; 88:062905 (2006).
44. Yuan GL, Or SW, Chan HLW. J Phys D Appl Phys ;40:1196–200 (2007).
45. Kumar M, Yadav KL. Appl Phys Lett; 91:242901(2007).
46. Yuan GL, Or SW, Wang YP, Liu ZG, Liu JM. Solid State Commun;138:76–81(2006).
47. Yuan GL, Or SW. J Appl Phys;100:024109 (2006).
48. Zhang S, Wang L, Chen Y, Wang D, Yao Y, Ma Y. J Appl Phys;111:074105 (2012).
49. Sun C, Wang Y, Yang Y, Yuan G, Yin J, Liu Z. Mater Lett;72:160-3 (2012).
50. Yuan G L, Or SW. Appl Phys Lett;88:062905 (2006).
51. Yuan GL, Or SW, Chan HLW. J Phys D Appl Phys;40:1196–200 (2007).
52. Yuan GL, Baba-Kishi KZ, Liu JM, Or SW, Wang YP, Liu ZG. J Am Ceram Soc;89:3136-9 (2006).
53. Yao Y, Liu W, Chan Y, Leung C, Mak C. Int J Appl Ceram Technol; 8:1246-53 (2011).
54. Teague, Gerson and James, Solid State Commun. **8**,1073 (1963).
55. Zavaliche, et al., Appl. Phys. Lett. **87**, 252902 (2005).
56. T. Zhao et al., Nature Mater. Vol. **5**, 823 (2006).
57. Zavaliche, et al. Appl. Phys. Lett. **87**, 182912 (2005).
58. Lane W. Martin et al., Nano Letters Vol. **8** No. 7 2050-2055 (2008).
59. Ying-Hao Chu et al., Adv. Mater. Vol. **19** 2662-2666 (2007).

60. Zheng H, Wang J, Lofland SE, Ma Z, Mohaddes-Ardabili L, Zhao T, et al. Science; 303:661-3 (2004).
61. Kumar A, Yadav KL. Mater Res Bull; 48(3):1312-15 (2013).
62. Feng M, Wang JJ, Hu JM, Wang J, Ma J, Li HB, et al. Appl Phys Lett;106(7):072901 (2015).
63. Mudinepalli VR, Song SH, Murty BS. Scripta Mater; 82:9–12 (2014).
64. Neaton JB, Ederer C, Waghmare UV, Spaldin NA, Rabe KM. Phys Rev B;71:014113 (2005).
65. Suryanarayana SV. Bull Mater Sci;17(7):1259-70 (1994).
66. Kimura T, Kawamoto S, Yamada I, Azuma M, Takano M, Tokura Y. Phys Rev B ;67(18):180401 (2003).
67. Oh YS, Crane S, Zheng H, Chu YH, Ramesh R, Kim KH. Appl Phys Lett;97(5):052902 (2010).
68. Calderon MJ, Liang S, Yu R, Salafranca J, Dong S, Yunoki S, et al. Phys Rev B ;84(2):024422 (2011).
69. Singh A, Pandey V, Kotnala RK, Pandey D. Phys Rev Lett;101(24):247602 (2008).
70. Yan L, Xing ZP, Wang ZG, Wang T, Lei GY, Li JF, et al. Appl Phys Lett;94:192902 (2009).
71. Ramana EV, Suryanarayana SV, Sankaram TB. Solid State Sci;12(5):956–62 (2010).
72. Lorenz M, Lazenka V, Schwinkendorf P, Bern F, Ziese M, Modarresi H, et al. J Phys D Appl Phys;47(13):135303 (2014).
73. Lazenka V, Lorenz M, Modarresi H, Bisht M, Rüffer R, Bonholzer M, et al. Appl Phys Lett;106(8):082904 (2015).
74. Yan L, Zhuo M, Wang Z, Yao J, Haberkorn N, Zhang S, et al. Appl Phys Lett 101(1):012908 (2012).
75. Yang HB, Zhang G, Chen HY, Li HM, Li Z. J Mater Sci ;26:3370–74 (2015).
76.Yang H, Zhang G, Han N. Mater Lett;145:91–94 (2015).
77. Li M, Ning M, Ma Y, Wu Q, Ong CK. J Phys D Appl Phys;40(6):1603-7 (2007).
78. Das R, Khan GG, Mandal K. J Appl Phys; 111(10):104115 (2012).
79. Palkar VR, Kundaliya DC, Malik SK, Bhattacharya S. Phys Rev B;69(21):212102 (2004).
80. Lee D, Kim MG, Ryu S, Jang HM, Lee SG. Appl Phys Lett; 86(22):222903 (2005).
81. Ismailzade IH, Ismailov RM, Alekberov AI, Salaev FM. Phys Stat Solid A;68(1):K81-5 (1981).
82. Singh A, Pandey V, Kotnala RK, Pandey D. Phys Rev Lett;101(24):247602 (2008).
83. Kumar M, Shankar S, Thakur OP, Ghosh AK. J Mater Sci; 26(3):1427-34 (2015).
84. Singh A, Gupta A, Chatterjee R. Appl Phys Lett;93(2):022902 (2008).
85. Chauhan Kumar SM, Chhoker S, Katyal SC, Singh H, Jewariya M, Yadav KL. Solid State Commun;152:525–29 (2012).
86. Jaiswal A, Das R, Maity T, Vivekanand K, Adyanthaya S, Poddar P. J Phys Chem C;114(29):12432–39 (2010).
87. Wu SM, Cybart SA, Yi D, Parker JM, Ramesh R, Dynes RC. Phys Rev Lett;110:067202 (2013).
88. Chu YH, Martin LW, Holcomb MB, Gajek M, Han S, He Q, et al. Nat Mater ;7(6):478–82 (2008).
89. Heron JT, Trassin M, Ashraf K, Gajek M, He Q, Yang SY, et al. Phys Rev Lett;107:217202 (2011).
90. Heron JT, Bosse JL, He Q, Gao Y, Trassin M, Ye L, et al. Nature ;516:370–3 (2014).
91. Heron JT, Schlom DG, Ramesh R. Appl Phys Rev;1:021303 (2014).
92. Hur N, Park S, Sharma PA, Ahn JS, Guha S, Cheong SW. Nature;429:392-5 (2004).
93. Gao F, Chen XY, Yin KB, Dong S, Ren ZF, Yuan F, et al. Adv Mater ;19:2889–92

(2007).
94. Li S, Nechache R, Davalos IAV, G. Goupil, L. Nikolova, M. Nicklaus, et al. J Am Ceram Soc; 96(10): 3155-62 (2013).
95. Zou J, Gong W, Ma J, Jiang J. J Nanosci Nanotechno;5(2):1304-11(2015).
96. Huang F, Wang Z, Lu X, Zhang J, Min K, Lin W, et al. Sci Rep;3:2907 (2013).
97. Arora M, Sati PC, Chauhan S, Singh H, Yadav KL, Chhoker S, Kumar M. Mater Lett; 96: 71-3 (2013).
98. Sakar M, Balakumar S, Saravanan P, Bharathkumar S. Nanoscale; 7(24): 10667-79 (2015).
99. Bhushan B, Basumallick A, Vasanthacharya NY, Kumar S, Das D. Solid State Sci; 12(7): 1063-9 (2010).
100. Arya GS, Kotnala RK, Negi NS. J Appl Phys; 113(4): 044107 (2013).
101. Hu Z, Wang Y, Dai J, Zhou D, Hu Y, Gu H, Baba-Kishi KZ. J Adv Dielect;1:325-30 (2011).
102. Chaudhuri A, Mandal K. J Magn Magn Mater; 353: 57-64 (2014).
103. Zhang H, Liu W, Wu P, Hai X, Guo M, Xi X, et al. Nanoscale;6(18):10831-8 (2014).
104. Mohan S, Subramanian B, Bhaumik I, Gupta PK, Jaisankar SN. RSC Adv;4(32):16871-8 (2014).
105. Nayek C, Thirmal C, Pa A, Murugavel P. Sci Eng: B; 199:121-4 (2015).
106. Albino GM, Perales-Pérez O, Renteria B, Galvez M, Guinel MJ. MRS Proceedings;1368 (2011).
107. Arora M, Kumar M. Ceram Int; 41(4):5705-12 (2015).
108. Yang C, Jiang JS, Wang CM, Zhang WG. J Phys Chem Solid;73(1):115-9 (2012).
109. Naeimi AS, Dehghan E, Khoshnoud DS, Gholizadeh A. J Magn Magn Mater ;393:502-7 (2015).
110. Yang C, Liu CZ, Wang CM, Zhang WG, Jiang JS. J Magn Magn Mater; 324(8):1483-7 (2012).
111. Guo R, Fang L, Dong W, Zheng F, Shen M. J Phys Chem C;114(49):21390-6 (2010).
112. Hu WW, Chen Y, Yuan HM, Li GH, Qiao Y, Qin YY, et al. J Phys Chem C ;115(18):8869–75 (2011).
113. Zou J, Gong W, Ma J, Jiang J. J Nanosci Nanotechno;5(2):1304-11 (2015).
114. Hasan M, Islam MF, Mahbub R, Hossain MS, Hakim MA. Mater Res Bull; 3: 179-86 (2016).
115. Ortiz-Quiñonez JL, Díaz D, Zumeta-Dubé I, Arriola-Santamar H, Betancourt I, Santiago-Jacinto P, Nava-Etzana N. Inorg Chem;2(18): 10306-17 (2013).
116. Huang F, Wang Z, Lu X, Zhang J, Min K, Lin W, et al. Sci Rep;3:2907 (2013).
117. Arora M, Sati PC, Chauhan S, Singh H, Yadav KL, Chhoker S, Kumar M. Mater Lett; 96: 71-3 (2013).
118. Muneeswaran M, Giridharan NV. J Appl Phys;115(21): 214109 (2014).
119. Wang B, Wang S, Gong L, Zhou Z. Ceram Int; 38(8): 6643-9 (2012).
120. Jaiswal A, Das R, Vivekanand K, Abraham P M, Adyanthaya S, Poddar P. Phys Chem C;14(5): 2108-15 (2010).
121. Goswami S, Bhattacharya D, Choudhury P. J Appl Phys;09(7):07D737 (2011).
122. Zhang XY, Lai CW, Zhao X, Wang DY, Dai JY. Appl Phys Lett; 87:143102 (2005).
123. Kim WH, Son JY. Mater Lett;121: 122-25 (2014).
124. Sun T, Pan Z, Dravid VP, Wang Z, Yu M, Wang J. Appl Phys Lett ;89(16):163117 (2006).
125. Reddy VA, Pathak NP, Nath R. J Alloys Compd;43:206-12 (2012).
126. Vijayasundaram SV, Suresh G, Kanagadurai R. Appl Phys A; 121(2): 681-8 (2015).
127. Selbach S M, Tybell T, Einarsrud M A, Grande T. Chem Mater;19(26): 6478-84 (2007).

128. Park TJ, Papaefthymiou GC, Viescas AJ, Moodenbaugh AR, Wong SS. Nano Lett;7(3):766–72 (2007).
129. Alina Manzoor, S. K. Hasanain, A. Mumtaz, M. F. Bertino, L. Franzel, J Nanopart Res, 14:1310 (2012).